

# Potential energy surface for the hydroperoxy and water ( $\text{HO}_2 \cdot \text{H}_2\text{O}$ ) radical complex

STEPHEN D. BELAIR, SABRE KAIS\* and JOSEPH S. FRANCISCO\*  
Department of Chemistry, Purdue University, West Lafayette, IN 47907, USA

(Received 23 January 2001; revised version accepted 30 July 2001)

A potential energy surface for the system of a hydroperoxy radical and a water molecule is presented. The surface was sampled using constrained density functional theory optimizations performed at the B3LYP level of theory using a 6-311++G(3df,3pd) basis set. The data points were fitted to an analytical function based on a common 4-point model for water and a 5-point model for the peroxy radical. A weighted least-squares fit of the parameters was performed using the nearest neighbour pivot method.

## 1. Introduction

Polar stratospheric clouds (PSCs) have been implicated in reactions responsible for the depletion of ozone in the Antarctic stratosphere [1–3]. It has been found that a significant fraction of the chemical transformations involving these clouds takes place in or on the surface of the cloud droplets. Such reactions are important because they augment gas phase processes and also facilitate reactions that do not normally take place in the gas phase [4–8]. Most of the reactants for these reactions are produced in the gas phase and then are either incorporated onto or into cloud droplets. In order to understand the impact of reactions taking place in or on cloud droplets, a number of laboratory efforts have been directed towards the measurement of sticking coefficients and mass accommodation coefficients, which are measures of the fraction of collisions of a gas phase species with a surface that result in the transport of the gas phase species into the condensed phase [9–12]. Uptake coefficients, which are the fraction of collisions that remove a species from the gas phase, also have been measured for a number of atmospheric species that play important chemical roles in the conversion of reservoir into photochemically labile species. Knowledge of the mass accommodation coefficient allows the rate of reaction in the cloud droplet to be determined. Most studies to date have focused on understanding how stable closed-shell species are incorporated into cloud droplets. There is a wealth of experimental and theoretical information on these systems [12]. However, less well understood is how open-shell species are incorporated into cloud droplets. Radicals play important roles in regu-

lating the propagating chemistry of the atmosphere. The transport of radicals into the condensed phase may account for a significant loss of reactants for gas phase radical processes, which could impact the partitioning of gas phase species in the atmosphere.

Recent field observations offer evidence for the uptake of radicals such as OH and  $\text{HO}_2$  by clouds [13–16]. In fact, recent aircraft observations of  $\text{HO}_2$ , OH, and  $\text{H}_2\text{O}_2$  in the upper troposphere show a significant imbalance in the  $\text{HO}_x$  chemical budget. This could possibly be corrected for by considering the conversion of  $\text{HO}_2$  in aerosols [16]. There are recent measurements of  $\text{HO}_2$  in fogs and clouds that show much lower  $\text{HO}_2$  concentrations than in clear sky [14, 15]. Laboratory and theoretical studies [17–22] do show that there is an unusually strong interaction of  $\text{HO}_2$  with  $\text{H}_2\text{O}$ . This interaction leads to the formation of an  $\text{HO}_2 \cdot \text{H}_2\text{O}$  complex. Laboratory studies [20] and recent theoretical studies [23] suggest that this complex can lead to the enhancement of rate processes in the gas phase. Nothing is known about what happens to  $\text{HO}_2$  in a water droplet or the mechanism for  $\text{HO}_2$  uptake by clouds.

Quantum calculations of the  $\text{HO}_2 \cdot \text{H}_2\text{O}$  complex have already been reported [22], but many of the atmospherically interesting questions involve an  $\text{HO}_2$  radical in the presence of a cloud droplet. A next logical step in theoretical studies of such clusters is to perform quantum calculations on  $\text{HO}_2 \cdot (\text{H}_2\text{O})_n$  clusters with  $n > 1$ . The difficulties with such calculations are the computational expense of quantum optimizations and the large number of possible configurations for such clusters. To make such calculations more practical, stochastic optimizations using classical potential energy functions can be performed first to determine good starting points for the quantum optimizations. The

\* Authors for correspondence. e-mail: kais@power1.chem.purdue.edu or jfrancis@purdue.edu

focus of this work is to construct an expression for the  $\text{HO}_2 \cdot \text{H}_2\text{O}$  potential energy surface that can be used to generate starting configurations for quantum calculations of small  $\text{HO}_2 \cdot (\text{H}_2\text{O})_n$  clusters.

## 2. Hydroperoxy and water ( $\text{HO}_2 \cdot \text{H}_2\text{O}$ ) radical complex

There have been several experimental studies that have examined the effect of water vapour on the kinetics of the  $\text{HO}_2$  gas phase reaction [17–20]. The existence of an  $\text{HO}_2 \cdot \text{H}_2\text{O}$  complex has been suggested to be involved in the kinetics, in which the rate of  $\text{H}_2\text{O}_2$  formation is enhanced by as much as a factor of three. Hamilton and Naleway [24] performed an *ab initio* calculation of the  $\text{HO}_2 \cdot \text{H}_2\text{O}$  complex using an STO-3G basis set. Their study did not use a fully optimized structure. In that structure, the oxygen of the  $\text{H}_2\text{O}$  and the hydrogen and the middle oxygen of the  $\text{HO}_2$  were constrained to be collinear. Also, the hydrogen bond axis was constrained to be on the  $\sigma_v$  plane of the water, which fixes the hydrogen atoms of the water to be symmetrical with respect to the hydrogen bond. Moreover, the authors did not perform a frequency calculation on their structure to verify that it was indeed a true minimum. Aloisio and Francisco [22], in a later theoretical study, found the Hamilton and Naleway structure to be a saddle point. In the Aloisio and Francisco optimized complex (figure 1), the hydrogen of the  $\text{HO}_2$  is weakly bound to the oxygen of the water. Also there is an attractive interaction between the terminal oxygen of the peroxy radical and one of the hydrogens on the water. This causes the complex to have a floppy five-membered ring-like structure, with the other hydrogen of the water out of the plane. The structure and vibrational frequencies were calculated at the B3LYP/6-311++G(3df,3pd) level of theory. Nelander [21] performed matrix isolation studies of the  $\text{HO}_2 \cdot \text{H}_2\text{O}$  complex in which vibrational frequencies were reported. Three

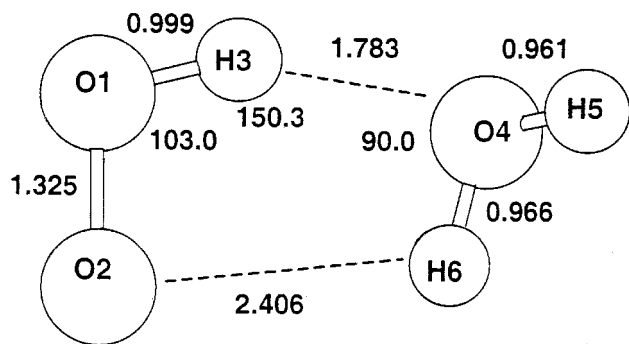


Figure 1. Fully optimized structure of the  $\text{HO}_2 \cdot \text{H}_2\text{O}$  complex (distances in Å and angles in deg).

major fundamental vibrational bands reported were 3236.2, 1479.3, and  $11.4 \text{ cm}^{-1}$ . The B3LYP/6-311++G(3df,3pd) calculations deviated by 2.1%, 5.2%, and 5.6% from the experimental values, respectively. Nelander suggested that the binding energy of the  $\text{HO}_2 \cdot \text{H}_2\text{O}$  complex is at least  $-6 \text{ kcal mol}^{-1}$ . Aloisio *et al.* [25] recently measured the equilibrium constant for the  $\text{HO}_2 + \text{H}_2\text{O} \rightleftharpoons \text{HO}_2 \cdot \text{H}_2\text{O}$  reaction, by measuring the loss of  $\text{HO}_2$  as a function of temperature and water vapour pressure. From the van't Hoff plot of the measured equilibrium constant, the binding energy was measured to be  $-8.6 \pm 3.8 \text{ kcal mol}^{-1}$ . The fully optimized structure of the complex using the B3LYP/6-311++G(3df,3pd) level of theory, as reported by Aloisio and Francisco [22], has a well depth  $-8.8 \text{ kcal mol}^{-1}$ . This calculated value is in very good agreement with the experimentally measured one.

## 3. Potential energy surface: data collection

The potential energy surface for the  $\text{HO}_2 \cdot \text{H}_2\text{O}$  complex was constructed by first performing quantum calculations to determine the potential energy of the complex in many configurations and then fitting these data to a simple analytical function. All quantum calculations were performed at the B3LYP level of theory with a 6-311++G(3df,3pd) basis set. We made these choices based on several factors. The first is that the calculations performed with the B3LYP/6-311++G(3df,3pd) combination [22] gave very good agreement with the experimental measurements [25]. Second, B3LYP is more computationally efficient than the other techniques used in the calculations cited. However, B3LYP has a reputation for not accounting properly for dispersion energy. So to ensure that this would not present a problem, MP2 check calculations were performed for several critical configurations of our system. Finally, the use of a large basis set can eliminate the need to perform basis set superposition error (BSSE) corrections. The BSSE was calculated at our lowest energy data point, using a centerpoise calculation, to be  $0.44 \text{ kcal mol}^{-1}$ . The uncorrected well depth of the rigid molecule complex was  $8.52 \text{ kcal mol}^{-1}$ . This is an error of 5.4%. The BSSE was also computed for several of the other optimized data points. These errors ranged from 2.4% to 6.3%. We believe this to be tolerable for our purposes.

Since we were constructing a potential energy surface for rigid molecule structures, it was first necessary to select a geometry for each, and since the potential energy was calculated as the difference between the energy of the complex and the sum of the equilibrium energies of the individual species, it was necessary also to compute the energy of those structures. The peroxy radical was fully optimized at the above level of theory,

and was found to have a geometry with bond distances  $r_{\text{OO}} = 1.3236 \text{ \AA}$ , and  $r_{\text{OH}} = 0.9751 \text{ \AA}$ , a bond angle  $\angle\text{HOO} = 105.4709^\circ$  and an energy of  $-150.9683 \text{ au}$ . All quantum calculations were performed using Gaussian 98 [27].

Because future work with this radical will include studies of  $\text{HO}_2 \cdot (\text{H}_2\text{O})_n$  clusters, it was necessary to pre-select a suitable water dimer potential, and in this way fix the geometry of our water molecule. We used the water dimer potential energy surface given by Matsuoka, Clementi and Yoshimine (MCY) [26]. The geometry of this water molecule has  $r_{\text{OH}} = 0.9572 \text{ \AA}$ ,  $r_{\text{OM}} = 0.2677 \text{ \AA}$  and  $\angle\text{HOH} = 104.5^\circ$ . At this level of theory, the isolated MCY water molecule has an energy of  $-76.4645 \text{ au}$ . We chose this function because, like the one we are constructing, it was derived for rigid molecules by fitting a simple functional form to potential energy data points that were generated with quantum calculations. The fact that it was fitted to a simple analytical function will reduce future computational costs. Also the MCY surface reproduces comparatively well structures of small clusters plus several properties of liquid water.

For all potential energy calculations, the  $\text{HO}_2$  was fixed in space with the central oxygen atom at the origin, the terminal oxygen atom on the negative  $z$  axis, and the hydrogen atom in the positive  $yz$  plane. For each optimization, the oxygen nucleus of the water molecule was fixed in space while its hydrogens were allowed to rotate freely (to within the constraints of the rigid water structure). In this way, the relative orientation of the two molecular species was optimized.

As the radical has a plane of symmetry, it was necessary to collect data in only half of the space. To achieve an even sampling of the space, data were collected with the oxygen atom of the water fixed at various distances along 17 different radial lines. The azimuth  $\theta$  and zenith  $\phi$  of each radial line are given in table 1. An additional radial line, directed to include the global minimum

Table 1. Radial lines used for data collection for the potential energy surface (angles in deg).

Line number	$\theta$	$\phi$	Line number	$\theta$	$\phi$
1	90	0	10	45	90
2	90	90	11	135	90
3	90	-90	12	45	-90
4	0	—	13	135	-90
5	180	—	14	45	45
6	45	0	15	45	135
7	135	0	16	-45	45
8	90	45	17	-45	135
9	90	-45	18	93.9	88.6

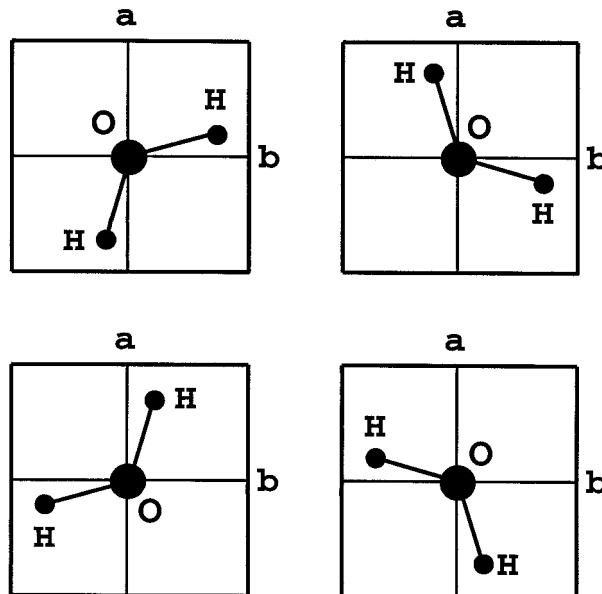


Figure 2. The four orientations of water in an  $ab$  plane. To avoid local minima, a series of single point calculations was carried out. For each of these the radical was fixed in space and the oxygen of the water was fixed at various positions. For each oxygen position, the energy of the system was computed for 12 different water orientations. The 4 orientations of water shown here represent the orientations in each of the  $XY$ ,  $XZ$ , and  $YZ$  planes.

(figure 1) was considered, but initial calculations indicated that the energy drop of the minimum from radial line 2 to this radial line 18 was only  $0.01 \text{ kcal mol}^{-1}$  for the geometry-constrained molecules. For this small change in energy, no additional information would be gained by sampling along this line, so it was not given further consideration.

Each data point used for the curve fitting was a constrained optimization as described above but, in order to avoid local minima, initially a series of single-point energy calculations was made. Single point energy calculations were performed along all radial lines at distances of 2.50, 2.75, 3.00, 3.25 and 3.50  $\text{ \AA}$ . At each point the water was placed in 12 different orientations. These are represented in figure 2 as four orientations in the  $ab$  plane. For the single-point calculations performed, the  $ab$  plane was each of the  $XY$ ,  $XZ$ ,  $YZ$  planes. It was observed that the single-point energy calculations near the equilibrium geometry, as shown in figure 1, missed the energy of the global minimum by more than  $2 \text{ kcal mol}^{-1}$ . For this reason, optimized potential energy data points rather than single-point potential energies were used for the fitting. The single-point values were used after the fitting to see if the curve could reproduce data that were not included in the fit.

From the single-point energy calculations, the lowest energy point along each radial line was identified. These points served as starting points for both distance and orientation for the constrained optimizations along each radial line. It was observed from these single point calculations that the potential energy along radial line 5 was purely repulsive. As it is our goal to construct a potential energy surface that can be used for obtaining starting points for quantum calculations, the inclusion of data from purely repulsive regions may not add useful information, and may require a more complicated function. For these reasons, data points along radial line 5 were not included in the fit. Because of this, it would be necessary to test the potential energy surface in order to see that it does indeed predict positive potential energy in this region.

After the optimization was performed from each starting point, the oxygen atom of the water was moved to distances  $\pm 0.1 \text{ \AA}$  along the radial line. Again, optimizations were performed. Optimizations at  $0.1 \text{ \AA}$  increments were continued at decreasing O1–O4 distances until the potential energy at a particular data point was greater than zero. Similarly, data were collected at increasing distances, but when the distance approached  $4 \text{ \AA}$  the resolution was changed to  $0.2 \text{ \AA}$  or  $0.5 \text{ \AA}$ , depending on the energy. The potential energies resulting from these constrained optimizations were the data points used to fit the parameters of the potential surface, and are plotted in figures 3 and 4. A total of 270 such points were collected.

#### 4. Selecting a functional form

The functional components of the MCY surface were used as an initial basis for selecting a functional form for this surface. All independent variables in the functional form used here were site–site distances, where each site corresponded either to a nucleus or a charge (or both).

For the MCY potential, the water molecule is represented by a four-point model. Three of these points are located at the nuclei, and the fourth point M7 is used to represent a shifting of the centre of negative charge away from the oxygen nucleus. The radical was modelled as a 5-point system with three sites located on the nuclei, and the other two representing centres of positive (M8) and negative (M9) charge. Figure 5 is a graphical representation of the 5-point model used for  $\text{HO}_2$  and the 4-point model of  $\text{H}_2\text{O}$ .

Since this surface is being fitted for rigid molecules, no interactions of sites on the same molecule were included in the functional form. Sites located on a nucleus were allowed to interact only with other nuclear sites, and sites containing a charge could only interact with other charge-containing sites. Charge–charge interactions were represented with a Coulombic function  $q_1q_2/r$ ,

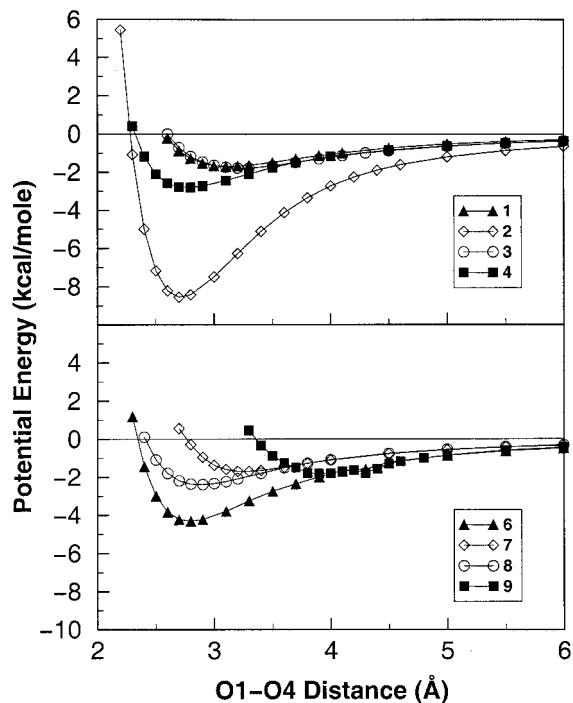


Figure 3. Potential energy data points for the complex as a function of the O1–O4 distance along radial lines 1–9. Potential energies were generated using B3LYP/6-311++ G(3df,3pd).

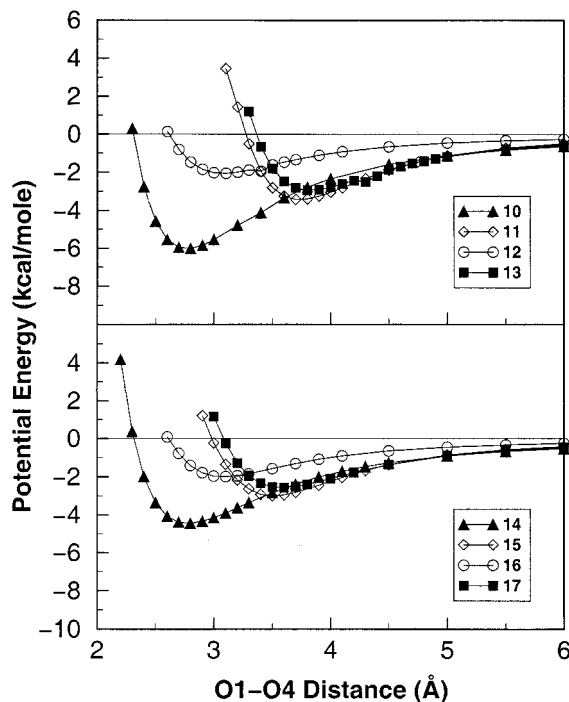


Figure 4. Potential energy data points for the complex as a function of the O1–O4 distance along radial lines 10–17. Potential energies were generated using B3LYP/6-311++ G(3df,3pd).

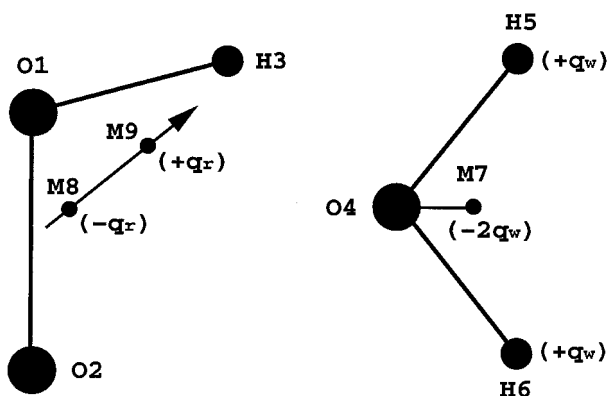


Figure 5. The 5-point model used for the peroxy radical and the 4-point model used for water. For charged sites, the magnitude of the charge is given in parentheses. For the curve fitting, points M8 and M9 were allowed to vary both in magnitude of charge and position, but were confined to the dipole moment vector. The charge and position of M7 were fixed at the MCY values.

where  $q_i$  is the charge on site  $i$ , and  $r$  is the distance between the sites. Interactions between nuclear sites were initially assigned one of two forms: for equivalent nuclei  $Ae^{-Br}$ , and for non-equivalent nuclei  $A_1e^{-B_1r} - A_2e^{-B_2r}$ , where  $A$  and  $B$  are free parameters. Sites interacting with the hydrogen atoms on the water were constrained to have the same set of parameters for both contributing terms. This portion of the potential is denoted as  $V^{\text{MCY}}$ :

$$\begin{aligned}
 V^{\text{MCY}} = & A_1e^{-B_1r_{14}} + A_2\{e^{-B_2r_{15}} + e^{-B_2r_{16}}\} \\
 & - A_3\{e^{-B_3r_{15}} + e^{-B_3r_{16}}\} + A_4e^{-B_4r_{24}} \\
 & + A_5\{e^{-B_5r_{25}} + e^{-B_5r_{26}}\} - A_6\{e^{-B_6r_{25}} + e^{-B_6r_{26}}\} \\
 & + A_7e^{-B_7r_{34}} - A_8e^{-B_8r_{34}} + A_9\{e^{-B_9r_{35}} + e^{-B_9r_{36}}\} \\
 & + q_wq_r\left\{-\frac{1}{r_{85}} - \frac{1}{r_{86}} + \frac{2}{r_{87}} + \frac{1}{r_{95}} + \frac{1}{r_{96}} - \frac{2}{r_{97}}\right\}. \quad (1)
 \end{aligned}$$

Initial attempts were made to fit the data to  $V^{\text{MCY}}$ . These attempts revealed that the  $V^{\text{MCY}}$  function was sufficient to fit the data points to the right of the minimum along each radial line. However, additional terms were needed to fit the data to the left of each minimum. Since there is no unique functional form to fit data such as these, we used a trial and error approach to decide the best integer value of the repulsive exponent. We found that an exponent of 12 gave the best fit. The functional form used to fit the data is

$$V = V^{\text{MCY}} + \sum_{i=1}^3 \sum_{j=4}^6 \left(\frac{C_{ij}}{r_{ij}}\right)^{12}. \quad (2)$$

## 5. Surface fitting

The nearest neighbour pivot method [28] with a Gaussian distribution as the pivoting distribution was used to perform the weighted least-squares fitting. A weighting factor was assigned to each point based on the energy of the point and relative to the point lowest in energy along the containing radial line. Points in the bottom quarter of each well were assigned a factor of 4, in the next highest quarter a factor of 2, and a factor of 1 elsewhere.

The value of each parameter was started at the value of the corresponding MCY value as reported by Wawak *et al.* [29]. The magnitude of the charge of the water  $q_w$  was fixed at  $13.07436 (\text{\AA} \text{ kcal mol}^{-1})^{1/2}$ , and the fourth point M7 was fixed at the same location and charge as the M of the MCY water molecule. The magnitude of the charge  $q_r$  of the radical was started at  $q_w$  but allowed to vary. Points M8 and M9 were allowed to move but were constrained to the line containing the dipole moment (figure 5). When the radical is fixed in space as described in § 3, the equation of the line containing the dipole moment of the radical is given by  $z = 0.855880y - 0.654888$ . M8 was started on the  $z$  axis and M9 was started near the hydrogen nucleus of the radical. Each  $C_{ij}$  in equation (2) was started at a value of 2.0.

Three constraints were implemented to ensure that the pivot method did not waste time searching in non-physical regions of the space. Calculations on the isolated radical showed that the relative spin densities on O1 and O2 are 0.3113 and 0.7077, respectively. For this, the first constraint required A4 to be larger than A1. Second, the dipole moment of the radical was constrained to point in the correct direction. Finally, each parameter was forced to be greater than zero, as the functional form was constructed in precisely this way.

Each attempt to fit the curve was performed with 500 probes. The starting Gaussian distribution for each parameter was set to a width of 20% of its initial value. A cooling factor of 95% was used, and the system was cooled every 40 cycles. Optimized values for the parameters are given in table 2. dM8 and dM9 are the distances from the  $z$  axis to the optimized positions of M8 and M9, respectively, along the dipole moment of the radical. The reported curve has unweighted and weighted least-squares deviation values of  $0.36677 \text{ kcal mol}^{-1}$  and  $0.36446 \text{ kcal mol}^{-1}$ , respectively. Figure 6 shows selected potential energy data points plotted with the corresponding values of the fitted potential energy surface.

## 6. Discussion and future work

A potential energy surface for the  $\text{HO}_2 \cdot \text{H}_2\text{O}$  system was constructed. The surface was sampled with 270

Table 2. The optimized values of the parameters for the potential energy surface. dM8 and dM9 are distances (in Å) of M8 and M9, respectively, from the  $z$  axis measured along the dipole moment vector. The units of all other parameters are assigned so that potential energies will be given in kcal mol<sup>-1</sup>. LSD and W-LSD are the unweighted and weighted least-squares deviations.

Parameter	Value	Parameter	Value
A1	0.949 691 12 × 10 <sup>6</sup>	A8	444.390 30
B1	5.264 614 9	B8	4.445 284 1
A1	1616.2752	A9	284.645 09
B2	6.471 018 5	B9	3.861 242 5
A3	16.479 198	$q_r$	18.851 321
B3	5.308 991 9	$q_w$	13.074 360
A4	3.301 283 5 × 10 <sup>6</sup>	dM8	0.976 553 2
B4	11.321 647	dM9	1.329 224 3
A5	2474.1314	$C_{14}$	1.215 552 0
B5	3.361 309 1	$C_{15} = C_{16}$	1.986 358 1
A6	537.023 06	$C_{24}$	2.697 955 7
B6	2.457 557 1	$C_{25} = C_{26}$	0.888 227 44
A7	2596.2080	$C_{34}$	0.151 554 25
B7	3.594 251 7	$C_{35} = C_{36}$	1.118 562 5
LSD	0.366 77	W-LSD	0.364 46

DFT calculations performed at the B3LYP level of theory using a 6-311++G(3df,3pd) basis set. The functional form for the surface was based on a 5-site model for the peroxy radical and a common 4-site model for water. All of the independent variables in the function were written as site-site distances. A weighted least-squares curve fitting was performed using the nearest neighbour pivot method. The reported curve had a weighted least-squares deviation value of 0.36446 kcal mol<sup>-1</sup>. Checking the surface against the single-point energy values showed that the surface was able to predict reasonably well the potential energy values in attractive regions of the space that were not included for the fitting. Also, calculations of the potential energy performed using this surface along radial line 5 were all repulsive, in agreement with the quantum chemistry calculations.

We plan to use this potential energy surface, in conjunction with the MCY water dimer surface, to study structures of HO<sub>2</sub> · (H<sub>2</sub>O)<sub>*n*</sub> clusters, and the effect that a water-rich environment can have on the chemistry of the hydroperoxy radical. Initial results for optimizing the HO<sub>2</sub> · (H<sub>2</sub>O)<sub>2</sub> cluster using this potential energy surface with the MCY surface were in very good agreement with *ab initio* calculations.

A study of these finite clusters may aid in understanding the interactions of the hydroperoxy radical with cloud droplets. Of particular interest is whether, after uptake, the radical remains on the surface of the

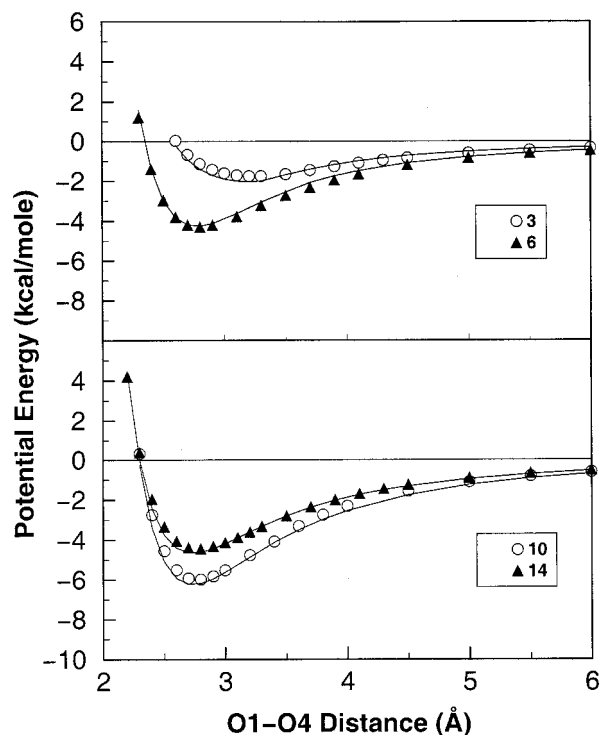


Figure 6. Plot of selected potential energy data (points) as a function of the O1-O4 distance, shown with the corresponding values of the fitted potential energy function (curves).

droplet, or is absorbed into the bulk, and what role this factor may play in altering its reactivity.

We would like to acknowledge the financial support of the National Science Foundation.

## References

- [1] SOLOMON, S., 1988, *Rev. Geophys.*, **26**, 131.
- [2] TOLBERT, M. A., 1994, *Science*, **264**, 527.
- [3] SOLOMON, S., GARCIA, R. R., ROWLAND, I. S., and WUEBBLE, D. J., 1986, *Nature*, **321**, 755.
- [4] MOLINA, L. T., MOLINA, M. J., STACHNIK, R. A., and TOM, R. D., 1985, *J. phys. Chem.*, **89**, 3779.
- [5] MOLINA, M. J., TSO, T. L., MOLINA, L. T., and WANG, F. C. Y., 1987, *Science*, **238**, 1253.
- [6] MOLINA, M. J., 1991, *Atmos. environ. A*, **25**, 2535.
- [7] ABBOTT, J. P. D., and MOLINA, M. J., 1991, *Geophys. Res. Lett.*, **19**, 461.
- [8] TOLBERT, M. A., ROSSI, M. J., MALHOTRA, R., and GOLDEN, D. M., 1987, *Science*, **238**, 1258.
- [9] HENSON, D. R., and RAVISHANKARA, A. R., 1991, *J. geophys. Res.*, **96**, 5081.
- [10] GARDNER, J. A., WATSON, L. R., ADEWAYI, Y. G., DAVIDOVITS, P., ZAHNISER, M. S., WARSNOP, D. R., and KLOB, C. E., 1987, *J. geophys. Res.*, **92**, 10887.
- [11] JAYNE, J. T., GARDNER, J. A., DAVIDOVITS, P., WARSNOP, D. R., ZAHNISER, M. S., and KLOB, C. E., 1990, *J. geophys. Res.*, **95**, 20559.

- [12] DEMORE, W. B., SANDER, S. P., GOLDEN, D. M., MOLINA, M. J., HAMPSON, R. F., KARYLO, C. J., and RAVISHANKARA, A. R., 1998, *Chemical Kinetics and Photochemical Data for Use in Stratospheric Modeling Evaluation*, #17, JPL Publication 98-1. (Pasadena, CA: California Institute of Technology).
- [13] MAULDIN, R. L., MADRONICH, S., FLOCKE, S. J., EISELE, F. L., FROST, G. J., and PREVOT, A. S. H., 1997, *Geophys. Res. Lett.*, **24**, 3033.
- [14] BRUNE, W. H. *et al.*, 1999, *Geophys. Res. Lett.*, **26**, 3077.
- [15] CANTRELL, C. A., SHETTER, R. E., GILPIN, T. M., CALVERT, J. G., EISELE, F. L., and TANNER, D. J., 1996, *J. Geophys. Res.*, **101**, 14653.
- [16] JAEGLE, L. *et al.*, 2001, *J. geophys. Res.*, in press.
- [17] HAMILTON, E., 1975, *J. chem. Phys.*, **63**, 3682.
- [18] COX, R. A., and BURROR, J. P., 1979, *J. phys. Chem.*, **83**, 2560.
- [19] LII, R. R., GROSE, R. A., SAUER, M. C., and GORDON, S., 1980, *J. phys. Chem.*, **84**, 813.
- [20] KIRCHER, C. C., and SANDER, S. P., 1984, *J. phys. Chem.*, **88**, 2082.
- [21] NELANDER, B., 1997, *J. phys. Chem. A*, **101**, 9092.
- [22] ALOISIO, S., and FRANCISCO, J. S., 1998, *J. phys. Chem. A*, **102**, 1899.
- [23] MOZURKEWICH, M., and BENSON, S. W., 1985, *Intl. J. chem. Kinetics*, **17**, 787.
- [24] HAMILTON, E. J., and NALEWAY, C. A., 1976, *J. phys. Chem.*, **80**, 2037.
- [25] ALOISIO, S., FRANCISCO, J. S., and FRIEDL, R. R., 2001, *J. phys. Chem.*, in press.
- [26] MATSUOKA, O., CLEMENTI, E., and YOSHIMINE, M., 1976, *J. chem. Phys.*, **64**, 1351.
- [27] FRISCH, M. J. *et al.*, 1998, Gaussian 98 Revision A.7 (Pittsburgh, PA: Gaussian, Inc.).
- [28] SERRA, P., STANTON, A. F., and KAIS, S., 1997, *Phys. Rev. E*, **55**, 1162.
- [29] WAWAK, R. J., WIMMER, M. M., and SCHERAGA, H. A., 1992, *J. phys. Chem.*, **96**, 5138.